J Therm Anal Calorim (2010) 99:905–909
DOI 10.1007/s10973-009-0489-2

# Martensitic transformation in Mn–Ni–Sn Heusler alloys

**R. Coll · L. Escoda · J. Saurina · J. L. Sánchez-Llamazares · B. Hernando · J. J. Suñol**

MEDICTA2009 Conference


**Abstract** Three magnetic shape memory alloys: $Mn_{50}Ni_{50-x}Sn_x$ ($x = 5$, 7.5, and 10) were produced as bulk polycrystalline ingots by arc melting. The structural austenite–martensite transformation was checked by calorimetry. The transformation temperatures decrease as increasing the Sn content. The same trend is found in the entropy and enthalpy changes related to the transformation. The control of the valence electron by atom *e*/*a* determines the transformation temperatures range in this kind of alloys and it is possible to develop alloys that can be candidates in applications as sensors and actuators. Furthermore, X-ray diffraction was performed to check the crystalline structure at room temperature.

**Keywords** Magnetic shape memory · DSC · Martensitic transformation

## Introduction

Ferromagnetic shape memory alloys exhibit ferromagnetic and shape memory effect simultaneously. The ferromagnetic shape memory effect can be controlled by temperature and stress, as well as by magnetic field. Their potential functional properties are: magnetic superelasticity [1], large inverse magnetocaloric effect [2], and large magnetoresistance change [3]. These properties make them of noteworthy interest for developing new thermal or magnetically driven actuators, sensors, and magnetic coolant for magnetic refrigeration [4].

Shape memory alloys exhibit a martensite phase transition. This transformation is a first order phase transition which takes place by the diffusionless shearing of the parent austenitic phase. By lowering the temperature a cubic high-temperature parent austenite phase transforms into a tetragonal, orthorhombic, or monoclinic martensite ordered by domains. Thermal analysis is useful to determine transformation temperatures in ferromagnetic alloys with structural transformations [5–9]. The transformation temperatures of shape memory alloys strongly depend on the composition and their values spread in a very wide range [10]. The mobility of the martensitic domains allows inducing large macroscopic deformations of the sample by applying an external stress. This deformation does not cost much energy since the crystal structure remains unmodified; only the domain walls move [11].

Among the alloys that exhibits magnetic shape memory effect, the most extensively studied are the Heusler alloys, defined as magnetic ternary intermetallic systems with $L2_1$ or B2 crystal structure. Their generic formula is $X_2YZ$. Here, X is usually a transition metal 3d (Fe, Co, Ni, Cu, Zn), 4d (Ru, Rh, Pd, Ag, Cd), or 5d (Ir, Pt, Au). The position of Y is usually occupied by 3d (Ti, V, Cr, Mn), 4d (Y, Zr, Nb), 5d (Hf, Ta) or by lanthanides (Gd, Tb, Dy, Ho, Er, Tm, Yb, Lu) or actinides (U). The Z is a group-B element: III-B (Al, Ga, In, Tl), IV-B (Si, Ge, Sn, Pb) or V-B (As, Sb, Bi). The most extensively studied Heusler alloys have those of the Ni–Mn–Ga system. However, to overcome some of the problems related with practical applications (such as the high cost of Gallium and the usually low martensitic transformation temperature) the search for Ga-free alloys has been recently attempted. In particular, by introducing In or Sn.

R. Coll · L. Escoda · J. Saurina · J. J. Suñol (✉)
GRMT.—University of Girona, Campus Montilivi s/n, Girona 17003, Spain
e-mail: joanjosep.sunyol@udg.edu

J. L. Sánchez-Llamazares · B. Hernando
Departamento de Física, Facultad de Ciencias, Universidad de Oviedo, Calvo Sotelo s/n, Oviedo 33007, Spain

Martensitic transformation in ferromagnetic Heusler $Ni_{50}Mn_{50-x}Sn_x$ alloys with $10 \leq x \leq 16.5$ was first reported by Sutou et al. [12]. Later, Krenke et al. studied phase transformations, magnetic and magnetocaloric properties of the Heusler $Ni_{50}Mn_{50-x}Sn_x$ alloy series with $5 \leq x \leq 25$ [3, 13]. Samples with $x = 13$ and 15, are ferromagnetic in the martensitic state undergoing a first order martensitic–austenitic structural transition at a temperature below the respective Curie points of both phases. Brown et al. [14] and Koyama et al. [15] reported on the structural and magnetoelastic behavior of the alloy $Ni_{50}Mn_{36}Sn_{14}$. Ni–Mn–Sn system is therefore of prospective importance as ferromagnetic shape memory alloy. In all the cases, alloys were produced as bulk polycrystalline ingots by arc melting followed by high temperature homogenization annealing. In this study, we analyze three alloys in the Ni–Mn–Sn system (by modifying the Sn content) in order to develop materials with a martensite–austenite transformation temperature range above, near, or below room temperature. These materials can be candidates for future applications as sensors or actuators.

## Materials and methods

As-cast pellets of nominal composition $Ni_{50}Mn_{50-x}Sn_x$ ($x = 5$, 7.5 and 10) were labeled as Sn5, Sn7.5, and Sn10, respectively. The alloys were prepared by Ar arc melting from 99.98% pure Ni, 99.98% pure Mn, and 99.999% pure Sn, using Bühler MAM-1 compact arc melter. Ingots were melted four times to ensure a good starting homogeneity. Annealing at 1,273 K was performed in order to obtain more homogeneous alloys.

The austenite–martensite structural transformation was checked by calorimetry. The cyclic experiments (heating–cooling) were recorded at 10 K/min under argon atmosphere. DSC scans above room temperature were performed in the DSC high temperature DSC modulus of the Setaram Setsys system and the DSC scan below room temperature was performed in the DSC 30 device of Mettler–Toledo working with a liquid nitrogen cooling system.

X-ray diffraction (XRD) analyses were performed at room temperature with a Siemens D500 X-ray powder diffractometer using Cu-K$\alpha$ radiation ($\lambda = 1.5418$ Å). Scanning was carried out in the interval $30° \leq 2\theta \leq 75°$ with a step increment of 0.05°.

## Results and discussion

To determine the thermal analysis conditions it is important the knowledge of crystal structure at room temperature. If the detected phase is cubic, the austenite–martensite transition must be found below room temperature. If the detected phase is orthorhombic, tetragonal or monoclinic, the austenite–martensite transformation must be found by heating the alloy. For it, XRD patterns were collected at room temperature, see Figs. 1, 2, and 3.

Alloys with Sn5 and Sn7.5 have an orthorhombic structure whereas alloy with Sn10 has a cubic $L2_1$ structure. Miller indexes were assigned with the aid of indexing programs as Treor and Dicvol. XRD lattice parameters are given in Table 1. The orthorhombic phase is the same in Sn5 and Sn10 alloys. Nevertheless, the relative peaks

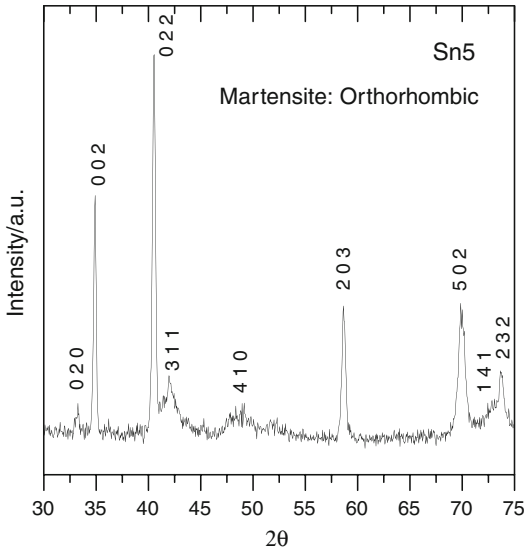


**Fig. 1** X-ray diffraction pattern at room temperature for $Mn_{50}Ni_{45}Sn_5$ alloy. The crystalline structure is orthorhombic

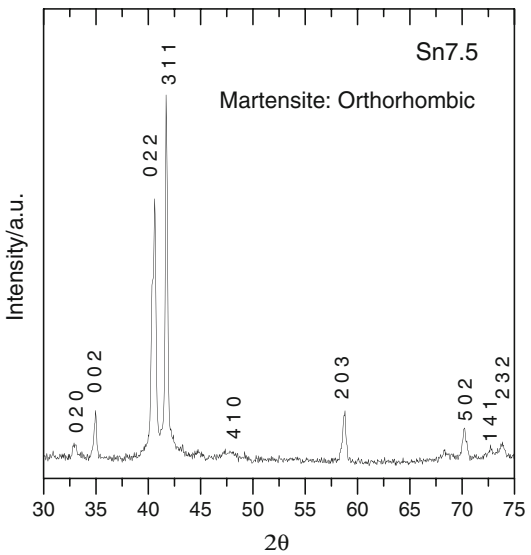


**Fig. 2** X-ray diffraction pattern at room temperature for $Mn_{50}Ni_{42.5}Sn_{7.5}$ alloy. The crystalline structure is orthorhombic

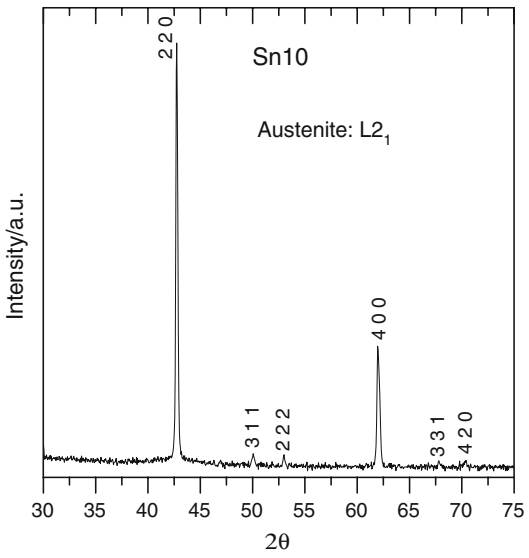


**Fig. 3** X-ray diffraction pattern at room temperature for $Mn_{50}Ni_{40}Sn_{10}$ alloy. The crystalline structure is cubic $L2_1$

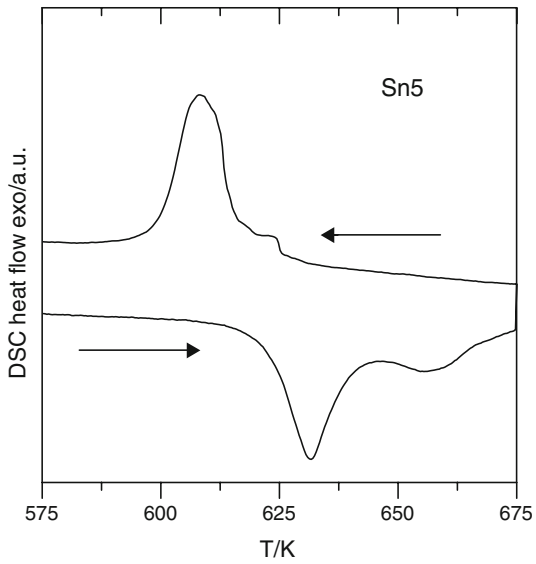


**Fig. 4** DSC cyclic scan for the alloy $Mn_{50}Ni_{45}Sn_5$ at a heating/cooling rate of 10 K/min. Arrows indicate cooling (*up*: martensite to austenite) and heating (*down*: austenite to martensite)

**Table 1** XRD lattice parameters calculated from diffraction patterns at room temperature

| Alloy | Crystalline structure | Lattice parameters/nm |
|---|---|---|
| Sn5 | Orthorhombic | $a = 0.7889(9)$ |
| | | $b = 0.5383(8)$ |
| | | $c = 0.5143(8)$ |
| Sn7.5 | Orthorhombic | $a = 0.7862(9)$ |
| | | $b = 0.5379(6)$ |
| | | $c = 0.5117(9)$ |
| Sn10 | Cubic $L2_1$ | $a = 0.5997(6)$ |

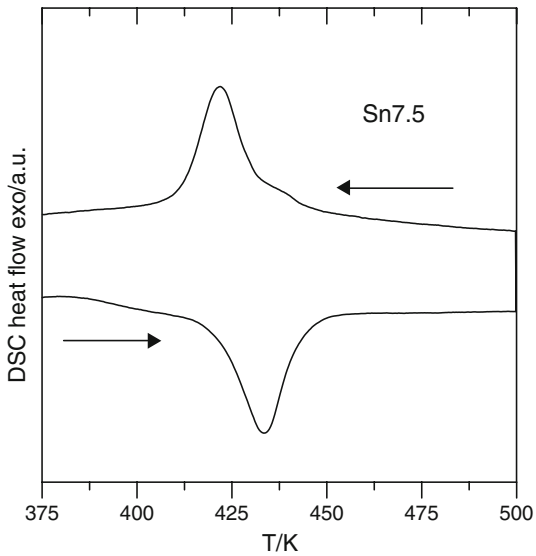


**Fig. 5** DSC cyclic scan for the alloy $Mn_{50}Ni_{42.5}Sn_{7.5}$ at a heating/cooling rate of 10 K/min. Arrows indicate cooling (*up*: martensite to austenite) and heating (*down*: austenite to martensite)

intensity is different. It is known that Heusler alloys sometimes present texture effects [16]. In Sn10 alloy, the peaks reflections indexed as 3 1 1 and 3 3 1 confirms the existence of the highly ordered $L2_1$ structure.

From XRD diffraction patterns it is clear that DSC scans of alloys Sn5 and Sn7.5 should be performed by heating from room temperature in order to detect the martensite–austenite transition (see Figs. 4, 5). Likewise, DSC scan of alloy Sn10 should be performed by cooling from room temperature (see Fig. 6). Really, cyclic experiments were done due to the hysteresis of the transformation. In alloys Sn5 and Sn7.5 two processes were found in the first cycle, perhaps due to a non complete homogenization of the annealed alloy. After several cycles this effect disappears. The characteristic transformations temperatures at which martensite start and finish ($M_s$ and $M_f$), and austenite start and finish ($A_s$ and $A_f$) are collected in Table 2. The hysteresis is due to the increase of the elastic and the surface energy during the martensite formation. Thus, the nucleation of the martensite implies supercooling. For it, it is determined the width of the hysteresis, $\Delta T$, as the difference the temperatures corresponding to the peak position. In this study, this parameter range between 12 and 23 K. The transformation region can be also characterized by the martensite transformation temperature $T_0$: the temperature at which the Gibbs energies of the martensitic and parent phases are equal [17].

$$T_o = \frac{1}{2}(M_s + A_f) \quad (1)$$

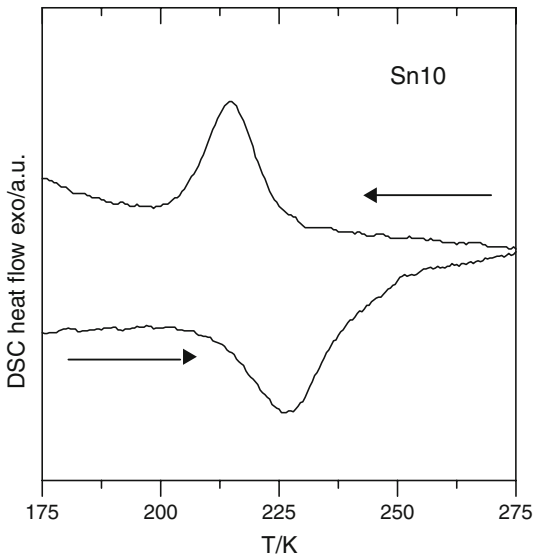


**Fig. 6** DSC cyclic scan for the alloy $Mn_{50}Ni_{40}Sn_{10}$ at a heating/cooling rate of 10 K/min. Arrows indicate cooling (*up*: martensite to austenite) and heating (*down*: austenite to martensite)

$T_o$ values are 646, 440, and 237 K for alloys Sn5, Sn7.5, and Sn10, respectively.

The transformation temperatures of shape memory alloys strongly depend on the composition and their values spread in a very wide range. Similar results were found in other NiMn(In,Sn) Heusler alloys [18, 19]. The average number of valence electrons by atom (*e*/*a*) is a parameter used to characterize these alloys. This concentration is calculated using the electron concentration of the outer shells for each chemical component of the Mn–Ni–Sn alloy as follows:

$$e/a = \frac{7x\ (\text{at.\%Mn}) + 10x\ (\text{at.\%Ni}) + 4x(\text{at.\%Sn})}{100} \qquad (2)$$

Here, the value of 7 is applied for manganese, in which the other electron shells are occupied by $3d^5 4s^2$, while for nickel the value becomes 10 from $3d^8 4s^2$ and for thin 4 from $5s^2 5p^2$. Consequently, the *e*/*a* values are 8.2, 8.05, and 7.9 for samples with 5, 7.5, and 10 at.%Sn, respectively. It is known that there is a linear correlation between the average number of valence electrons per atom and the martensite start temperature [20]. $M_s$ increases with increasing *e*/*a*. The same behavior is found in this study. Thus, the control of *e*/*a* determines the transformation temperatures range in this kind of alloys and it is possible to develop alloys with the desired transformation temperatures as candidates for applications as sensors and actuators.

The entropy ($\Delta S$) and enthalpy ($\Delta H$) changes of the structural transformations are calculated from calorimetry data [21] using the relationships

$$\Delta H = \int_{T_i}^{T_f} \left[ \left( \frac{dQ}{dt} \right) \left( \frac{dT}{dt} \right)^{-1} \right] dT \qquad (3)$$

and

$$\Delta S = \int_{T_i}^{T_f} \left[ \frac{1}{T} \left( \frac{dQ}{dt} \right) \left( \frac{dT}{dt} \right)^{-1} \right] dT \qquad (4)$$

where $T_i$ and $T_f$ are the temperature limits of integration.

The entropy and enthalpy change values are also included in Table 2. The values decrease as increasing (decreasing) the Sn content (*e*/*a* number). The same trend was found by other authors [22]. It has been argued [21] that the electron contribution to $\Delta S$ is negligible and that character of the *e*/*a* dependence is related to a magnetic contribution that relies on the difference between the magnetic exchange below and above $M_s$. The thermal behavior was not modified by consecutive cycles (only the minor effect of alloys Sn5 and Sn7.5 disappears).

Further studies are in course (in the Ni–Mn–Sn system) in order to understand better the role of the variability of synthesis conditions and the effect of thermal annealing on the microstructure, phase transformation, and magnetic properties.

## Conclusions

Three Heusler shape memory alloys: $Mn_{50}Ni_{45}Sn_5$, $Mn_{50}Ni_{42.5}Sn_{7.5}$, and $Mn_{50}Ni_{40}Sn_{10}$ were produced as bulk polycrystalline ingots. As determined from the analysis of X-ray diffraction patterns at room temperature, alloys with Sn5 and Sn7.5 has a textured orthorhombic martensite structure whereas alloy with Sn10 has a martensite cubic $L2_1$ structure.

The characteristic transformations temperatures at which martensite start and finish ($M_s$ and $M_f$), and austenite

**Table 2** Structural transition temperatures and the associated characteristic thermal parameters: h and c indicates calculated from heating or cooling, respectively

| Alloy | $M_s$/K | $M_f$/K | $A_s$/K | $A_f$/K | $\Delta T$/K | $T_0$/K | $\Delta H$/J mol$^{-1}$ | $\Delta S$/J mol$^{-1}$ K$^{-1}$ |
|---|---|---|---|---|---|---|---|---|
| Sn5 | 625 | 597 | 618 | 667 | 23 | 646 | 148 (h) 171 (c) | 0.24 (h) 0.28 (c) |
| Sn7.5 | 436 | 407 | 389 | 444 | 12 | 440 | 105 (h) 118 (c) | 0.24 (h) 0.27 (c) |
| Sn10 | 228 | 202 | 205 | 246 | 13 | 237 | 24 (h) 22 (c) | 0.11 (h) 0.10 (c) |

start and finish ($A_s$ and $A_f$) and the thermodynamic martensite transformation temperature ($T_o$) strongly depend on the composition and their values spread in a very wide range. As expected, $M_s$ increases as increasing *e/a* (valence electron by atom). Thus, the *e/a* control permit the development of alloys with the desired transformation temperatures. Likewise, the entropy and enthalpy change related to the transformation decrease as decreasing *e/a*.

**Acknowledgements** FICYT is acknowledged by J.L.S.LL (COF07-013). This study has been supported by the Spanish MEC under projects MAT2006-13925-C02-01 and MAT2006-13925-C02-02.

## References

1. Krenke T, Duman E, Acet M, Wassermann EF, Moya X, Mañosa L, et al. Magnetic superelasticity and inverse magnetocaloric effect in Ni–Mn–In. Phys Rev B. 2007;7575:104414.
2. Pons J, Chernenko VA, Santamarta R, Cesari E. Crystal structure of martensitic phases in Ni–Mn–Ga shape memory alloys. Acta Mater. 2000;48:3027–38.
3. Koike K, Ohtsuka M, Honda Y, Katsuyama H, Matsumoto M, Itagaki K, et al. Magnetoresistance of Ni–Mn–Ga–Fe ferromagnetic shape memory. J Magn Magn Mater. 2007;310:996–8.
4. Marioni MA, O'Handley ROC, Allen SM, Hall SR, Paul DJ, Richard ML, et al. The ferromagnetic shape–memory effect in Ni–Mn–Ga. J Magn Magn Mater. 2005;290:35–41.
5. Bouabdallah M, Cizeron G. Differential scanning calorimetry of transformation sequences during slow heating of Cu–Al–Ni shape memory alloys. J Therm Anal Calorim. 2002;68:951–6.
6. Auguet C, Isalgué A, Lovey FC, Pelegrina JL, Ruiz S, Torra V. Metastable effects on martensitic transformation in SMA. J Therm Anal Calorim. 2007;89:537–42.
7. Sepúlveda A, Muñoz R, Lovey FC, Auguet C, Isalgué A, Torra V. Metastable effects on martensitic transformation in SMA. J Therm Anal Calorim. 2007;89:101–7.
8. Bonastre J, Escoda L, González A, Saurina J, Suñol JJ. Influence of Ni content on Fe–Nb–B alloy formation. J Therm Anal Calorim. 2007;88:83–6.
9. González A, Bonastre J, Escoda L, Suñol JJ. Thermal analysis of Fe (Co, Ni) based alloys prepared by mechanical alloying. J Therm Anal Calorim. 2007;87:255–8.
10. Bhobe PA, Priolkar KR, Nigam AK. Room temperature magnetocaloric effect in Ni–Mn–In. Appl Phys Lett. 2007;91:242503.
11. Pierre J, Karla L, Kaczmarska K. Giant magnetoresistance in Heusler-type rare earth and 3d semiconductors. Physica B. 1999; 261:845–6.
12. Sutou Y, Imano Y, Koeda N, Omori T, Kainuma R, Ishida K, et al. Magnetic and martensitic transformations of NiMnX (X = In, Sn, Sb) ferromagnetic shape memory alloys. Appl Phys Lett. 2004;85:4358.
13. Krenke T, Duman E, Acet M, Wassermann EF, Moya X, Mañosa L, et al. Inverse magnetocaloric effect in ferromagnetic Ni–Mn–Sn alloys. Nat Mater. 2005;4:450–4.
14. Brown PJ, Gandy AP, Ishida K, Kainuma R, Kanomata T, Neumann KU, et al. The magnetic and structural properties of the magnetic shape memory compound Ni2Mn1.44Sn0.56. J Phys Condens Matter. 2006;18:2249–59.
15. Koyama K, Watanabe K, Kanomata T, Kainuma R, Oikawa K, Ishida K. Observation of field-induced reverse transformation in ferromagnetic shape memory alloy Ni50Mn36Sn14. Appl Phys Lett. 2006;88:132505.
16. Sánchez-Llamazares JL, Sánchez T, Santos JD, Pérez MJ, Sánchez ML, Hernando B, et al. Martensitic phase transformation in rapidly solidified Mn50Ni40In10 alloy ribbons. Appl Phys Lett. 2008;92:012513.
17. Kaufman L, Hullert M. Thermodynamics of martensite transformation. In: Olson GB, Owen WS, editors. Martensite. Cambridge: ASM International; 1992. p. 41–58.
18. Santos JD, Sánchez T, Alvarez P, Sánchez ML, Sánchez-Llamazares JL, Hernando B, et al. Microstructure and magnetic properties of Ni50Mn37Sn13 Heusler alloy ribbons. J Appl Phys. 2008;103:07B326.
19. Hernando B, Sánchez-Llamazares JL, Santos JD, Escoda L, Suñol JJ, Varga R, et al. Thermal and magnetic field-induced martensite-austenite transition in Ni50.3Mn35.3Sn14.4 ribbons. Appl Phys Lett. 2008;92:042504.
20. Chernenko VA. Compositional instability of beta-phase in Ni–Mn–Ga alloys. Scr Mater. 1999;40:523–7.
21. Krenke T, Acet M, Wassermann EF, Moya X, Mañosa L, Planes A. Ferromagnetism in the austenitic and martensitic states of Ni–Mn–In alloys. Phys Rev B. 2006;73:174413.
22. Krenke T, Acet M, Wassermann EF, Moya X, Mañosa L, Planes A. Martensitic transitions and the nature of ferromagnetism in the austenitic and martensitic states of Ni–Mn–Sn alloys. Phys Rev B. 2005;72:014412.